Coexistence of fcc- and bcc-like crystal structures in ultrathin Fe films grown on Cu(111)

A. Biedermann
Institut für Materialphysik, University of Vienna, A-1090 Vienna, Austria

W. Rupp, M. Schmid, and P. Varga
Institut für Allgemeine Physik, Vienna University of Technology, A-1040 Vienna, Austria
(Received 2 June 2005; revised manuscript received 23 December 2005; published 25 April 2006)

We report on bcc-like phases in ultrathin Fe films grown by thermal deposition on Cu(111) previously thought to consist exclusively of fcc phases distinguished only by their magnetic order. Our scanning tunneling microscopy and spectroscopy data together with published x-ray photoelectron diffraction results [M. T. Kief and W. F. Egelhoff, Jr., Phys. Rev. B **47**, 10785 (1993)] provide us with sufficient detail to deduce the film structure. Two growth regimes are considered: (1) films with 1–2 monolayer average thickness grown near 200 K, which nucleate as bcc-like bilayer islands: Larger islands show bcc-like fringes coexisiting with an fcc center domain; i.e., the bcc-like phase is stable only within a certain distance to a step edge. The presence of a bcc-like bilayer phase provides a straightforward explanation for the ferromagnetism previously observed in these films. In addition we find that the bcc-like phase can be promoted by H adsorption at 80 K. The bcc domains form "displacement vortex" structures to simultaneously minimize film stress and interface energy. (2) In films grown at room temperature, between pseudomorphic fcc areas, we observe a more ideal but still strained bcc phase in regions with a local thickness of at least 4 monolayers. Also in this growth regime, the fcc-bcc transformation is facilitated by step edges, which are abundant due to the imperfect layer-by-layer growth.

DOI: 10.1103/PhysRevB.73.165418 PACS number(s): 68.55.−a, 64.70.−p, 75.70.−i, 81.30.−t

I. INTRODUCTION

For many years now, ultrathin Fe films on Cu have been scrutinized in order to explore the interaction of the crystal structure with the magnetic state of the Fe atoms [e.g., Refs. 1–12 for Fe/Cu(100) and Refs. 13–18 for Fe/Cu(111)]. So far these films have been approached with the assumption that they are either nearly relaxed bcc (ground state of bulk Fe) or strained fcc ("pseudomorphic"). Most theories predict some form of antiferromagnetic order for fcc Fe.[19–24] Frequently encountered high-moment ferromagnetism in ultrathin Fe films thought to be fcc was interpreted as the formation of a ferromagnetic fcc-like phase.[19,20,25]

Our scanning tunneling microscopy (STM) images of ultrathin Fe films grown on Cu(100),[26–28] however, have revealed a class of strongly strained bcc phases as the likely source of this ferromagnetism. The influence of the fcc Cu substrate leads to a strong distortion of the bcc film structure, which improves the lattice matching at the interface. Apparently, bcc Fe films are particularly tolerant for substrate-induced distortions along pathways towards the fcc structure. This may be related to the small energy difference and small barrier between the fcc and bcc phases.[29] The result is a variety of bcc-like, highly-fcc-lattice-matched structures, which are not easily identified by surface averaging methods. On the (100)-oriented Cu substrate, for instance, a very tight martensitic folding of a strained bcc phase termed "nanomartensite" occurs, which has the same layer atom density as the fcc phase and therefore forms without interlayer mass transport.[27] Besides the obvious driving force, the increased stability of the bcc phase at low temperatures, also a strong bcc-stabilizing finite-thickness effect is seen in very thin Fe/Cu(100) films below 4–5 monolayer (ML) local thickness:[28] The lower average coordination number at the surface and interface apparently decreases the total energy of the bcc phase relative to the fcc phase and stabilizes the bcc-like phase even in Fe/Cu(100) films only 2 ML thick.

In this article we demonstrate that similar bcc-like phases also form in Fe/Cu(111) films but that they are more complex than those observed in the Fe/Cu(100) system. Fe films grown on Cu(111) significantly below 300 K are characterized by a three-dimensional (3D) growth mode, which renders experiments on this substrate more difficult compared to the Fe/Cu(100) system. Nevertheless, by using x-ray photoelectron diffraction (XPD) as a probe for local bond directions, the local atomic structure could be determined at both room temperature and below.[16,30] According to these experiments, the films show a bcc-like layer stacking (1) independent of thickness when grown at 80 K or (2) above an average thickness of 2–3 ML when grown at 300 K, and are therefore predominantly fcc only if less than 2–3 ML thick and grown at room temperature.[16,30]

Even though at 300 K the films grow in an imperfect layer-by-layer mode, they nucleate as a bilayer. Fe monolayers are virtually absent in films grown by "classic" thermal evaporation. Recently, this limitation could be overcome by pulsed laser deposition[31–33] (PLD) at temperatures near 200 K leading to a layer-by-layer like morphology starting with a monolayer. This modification of the growth mode, however, seems to be inseparably linked to intermixing with the Cu substrate, presumably due to energetic Fe particles, preventing the growth of pure Fe monolayers and bilayers by PLD.[33] Also, the island density and therefore step density are higher compared to thermally grown films.[32,33] In the litera-

ture, isotropic fcc structures are proposed for the PLD films on the basis of a structural analysis by low-energy electron diffraction (LEED).[31,32]

Measurements of the film magnetization[31,34] show a different thickness dependence for the thermally deposited (TD) films and those grown by PLD, both at 220 K. While the TD films show a monotonic, initially weak and clearly overlinear increase of the magnetization with increasing thickness, the PLD films show a very high, bulklike linear increase of the magnetization below 2 ML followed by a sudden decrease of the magnetization with increasing thickness around 2–3 ML thickness. The different magnetization values below 2 ML thickness for PLD and TD films have been attributed to the presence of high- and low-moment ferromagnetic fcc-like phases, respectively.[31,34]

The presentation of our results is preceded by a section describing experimental details and a short section introducing the crystallography of the fcc-bcc transition in ultrathin Fe/Cu(111) films. The results of our experiments are presented in three parts with the first describing growth and structure of the initial Fe islands near 200 K, where we find that bcc-like phases are present already at submonolayer coverage, the second describing the H_2-induced transformation of the bilayer island structure at 80 K, and the third describing the fcc to bcc conversion in films grown at 300 K, which starts at a critical local thickness of 4 ML. In the final section, our model of the film structure is discussed in detail and put into context with recently published experimental and theoretical work.

II. EXPERIMENT

The measurements were done using a low-temperature (LT) STM mounted inside of cryoshields cooled by a bath cryostat filled with liquid N_2 (Omicron LT-STM) and a room temperature (RT) STM (Omicron Micro-STM). Both microscopes were operated with electrochemically etched W tips conditioned by sputtering with Ar^+ under UHV conditions. Both STM systems are equipped with an Auger electron spectroscopy (AES) system. The RT-STM chamber also provides a LEED system.

The pressure during evaporation of the films in the preparation chambers is typically below 1×10^{-10} mbar, during measurement in the separate STM chamber of the RT-STM system in the 10^{-11} mbar range, and in the STM chamber of the LT system around 1×10^{-11} mbar.

The Cu(111) single crystal was typically sputtered with 2-keV Ar^+ ions and annealed at 870 K for 10 min. The films were grown by evaporation from an Fe wire using an electron bombardment evaporator. The emission of ions was suppressed by applying +1.5 kV to the exit electrode of the evaporator. The deposition rate of 0.5–1 ML/min was calibrated by a quartz crystal microbalance. After deposition the film thickness was checked by quantitative AES.[35]

In all hydrogen adsorption experiments, hydrogen dosing was done by backfilling the LT-STM chamber to the desired pressure with the sample at 80 K. The langmuir dose unit used ($1\ \mathrm{L}=10^{-6}$ Torr sec) is based on the true pressure, which for H_2 is the pressure measured by the N_2-calibrated ionization gauge in Torr multiplied by 2.2. Dosing was done through circular holes in the cryostat shields connecting the inside (sample surface) and outside of the cryostat shields. We remark that a more efficient hydrogen adsorption on the surfaces inside the cryostat shields may lead to a reduced actual hydrogen dose near the sample.

Some of the atomically resolved STM images show inverse corrugation; i.e., the atom positions are indicated by corrugation minima rather than maxima as intuitively expected. This is not unusual for the Fe surface and can be explained by the extremely low corrugation of the Fermi edge local density of states of the undisturbed Fe surface in the first place and the strong tip-sample interactions, which are thought to enhance or even produce the actually observed (positive or negative) atomic contrast.[36] We often invert the gray scale of such images for convenience and add a respective note in the figure caption.

Scanning tunneling spectroscopy (STS) was carried out by measuring *I-V* curves followed by numerical differentiation. In order to visualize the spatial distribution of the various phases (chemical and structural) we employ a simple classification of the spectra: Reference spectra are defined by averaging over spectra in small regions which show clearly distinct spectral features. These typically two to four reference spectra are then used to classify the entire image by determination of the best-fit reference spectrum for each pixel. The results are surface fractions of each phase and spectra averaged over the entire area covered by a given phase.

STS is also used to determine whether Cu is present on the surface [cf. Ref. 28 for the Fe/Cu(100) system]. We find that the image contrast between Fe and Cu is larger than the contrast between fcc- and bcc-like Fe under most tunneling conditions. In this article, all images of films grown at 200 K show Fe surfaces virtually free of Cu. Films grown at or annealed to temperatures close to 300 K may be partially Cu covered, in particular near and at substrate step edges; i.e., film surfaces may contain significant amounts of copper in regions of high substrate step density.

Finally a few remarks on the preparation parameters heading many figures and appearing in the text: (1) The film thickness values in monolayers are average values unless explicitly labeled as "local" thickness values. (2) Most films were grown at one temperature and imaged at another. The respective values occupy positions 2 and 3 in the figure headers.

III. fcc-bcc TRANSFORMATION ON fcc(111) SUBSTRATES

The fcc (111) to bcc (110) transformation can be thought to consist of two steps [Fig. 1(a)]. In a first step, the stacking of the atomic layers is changed from threefold hollow site for fcc (111) films to bridge site. This is equivalent to an out-of-plane shear deformation of $\approx19°$ [Fig. 1(b)]. The second step, a 10.5° in-plane shear deformation, completes the transformation to the bcc (110) structure, leading either to the Kurdjumov-Sachs[37] (KS) or to the Nishiyama-Wassermann[38] (NW) orientation, which differ only by a rigid 5.3° rotation of the film relative to the substrate.

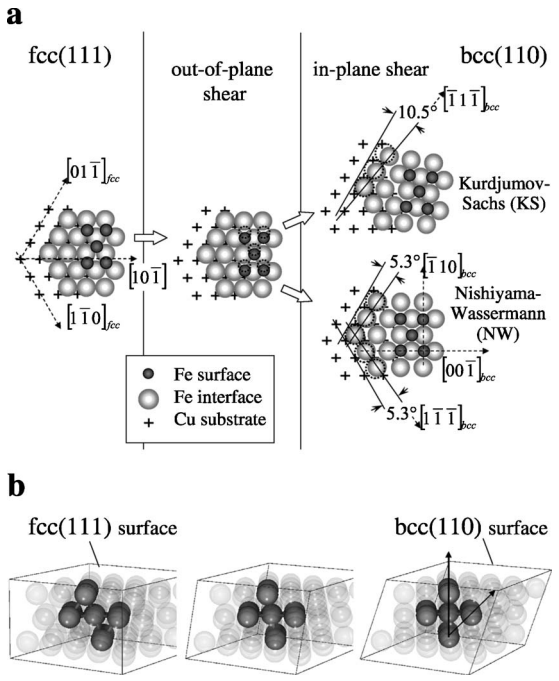

FIG. 1. fcc-bcc transformation of pseudomorphic fcc Fe films on an fcc (111) substrate. (a) Top view with consecutive out-of-plane and in-plane shear deformations. The dotted circles indicate atom locations before the respective shear strain is applied. In the Kurdjumov-Sachs (KS) orientation one of the two close-packed rows of the bcc (110) surface is aligned with a close-packed row of the fcc substrate. In the Nishiyama-Wassermann (NW) orientation both close-packed rows of the bcc (110) film are symmetrically misaligned with respect to the close-packed rows of the fcc substrate. (b) Side view of the fcc-bcc transformation (substrate not shown) with in-plane and out-of-plane shear simultaneously applied, demonstrating the dominant out-of-plane shear deformation of ≈19°. The body-centered tetragonal cell that becomes cubic in the bcc product is highlighted. The arrows indicate the ⟨110⟩ and ⟨100⟩ forward-scattering directions used in Refs. 16–18 to identify the bcc phase by XPD.

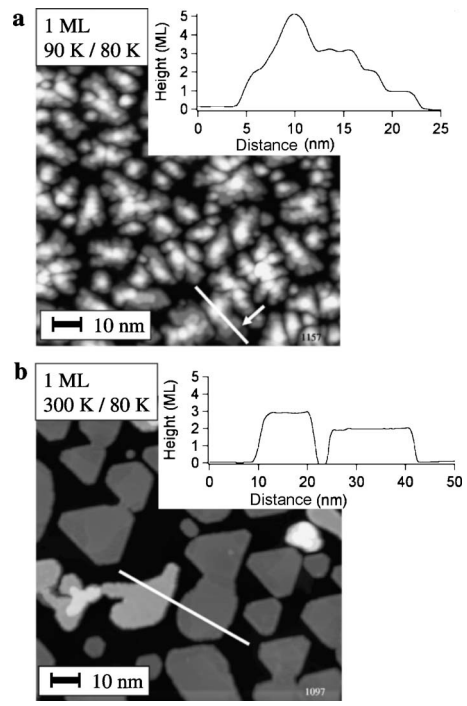

FIG. 2. STM images of 1-ML Fe films grown on Cu(111) and representative line profiles along the lines in the images. (a) The growth mode at 90 K is fully three dimensional, producing narrow pyramidal islands. The arrow indicates a small island part where the first monolayer is exposed (better visible in line profile). (b) Films grown at 300 K consist predominantly of bilayer islands. Tunneling conditions are −1 V sample voltage and 1 nA tunneling current. The image header of this and most other figures indicates the average film thickness, growth, and imaging temperatures.

In Fe/Cu(111) films we find bcc-like phases which show an incomplete second transformation step with in-plane shear deformations of ≈3° and ≈7°, which we term KS-3° and KS-7°. Ideal bcc would be "KS-10.5°" in this notation.

For the classification of a structure as "fcc-like" or "bcc-like," we calculate the strain energy of a given structure, assuming linear elasticity, with the fcc or bcc lattice as the reference state. For the bcc-like structures occurring in the Fe/Cu(100) or Fe/Cu(111) films, the linear strain energy is below 100 meV/atom if considered as strained bcc structure (cf. Sec. V B), compared to several 100 meV/atom if considered as strained fcc structure.

IV. RESULTS

A. Clean 1–2 ML Fe films grown at 200 K

1. STM of bilayer and pyramidal islands

For a substrate temperature of 90 K, we observe the growth of pyramidal islands [Fig. 2(a)] sometimes showing single Fe monolayers at their basis [arrow in Fig. 2(a)]. In contrast, films of similar average thickness grown at 300 K consist predominantly of corner-truncated triangular bilayer or trilayer islands [Fig. 2(b)]. These films, however, are problematic because of morphology-dependent Cu segregation (cf. Sec. II).

Cu segregation is absent at intermediate temperatures around ≈200 K where we observe the coexistence of bilayer and pyramidal islands [Fig. 3(a)]. While the pyramidal islands grown at 200 K are similar to those grown at 100 K, the bilayer islands grown at 200 K are more irregularly shaped than those grown at 300 K. This mixed 3D and bilayer growth is problematic if a well-defined morphology is required, which is important in particular for surface averaging experiments. For STM experiments, however, it is an advantage as different local growth modes can be studied side by side in an image or STS data set. For this reason and also for compatibility with previous experiments focusing on the magnetic structure[31] we have selected this temperature range also in many of the experiments presented here.

By increasing the contrast on the bilayer surface in the STM image, regions of reduced apparent height (appearing darker) are revealed in the center of larger bilayer islands [Fig. 3(b)]. Before we present evidence of the true nature of the two phases, we temporarily label them as "bright" and "dark" phase. By sorting the various islands with respect to

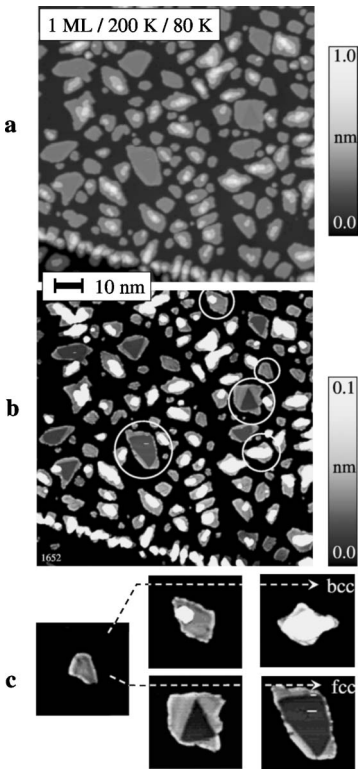

FIG. 3. STM image of a 1-ML film deposited at 200 K substrate temperature. (a) Original image: two different classes of islands can be distinguished: bilayer islands with a larger footprint and narrow, pyramidal islands, showing additional 2–3 atomic levels. (b) Same image with the gray scale adjusted to enhance the contrast for the second monolayer. (c) Different islands of increasing size (circles in overview image) are interpreted as stages of the island evolution: very small bilayer islands always appear "bright" and either evolve towards the pyramidal form (3D growth) or remain flat but develop a "dark" phase in their center region. Tunneling conditions: −0.1 V, 0.3 nA.

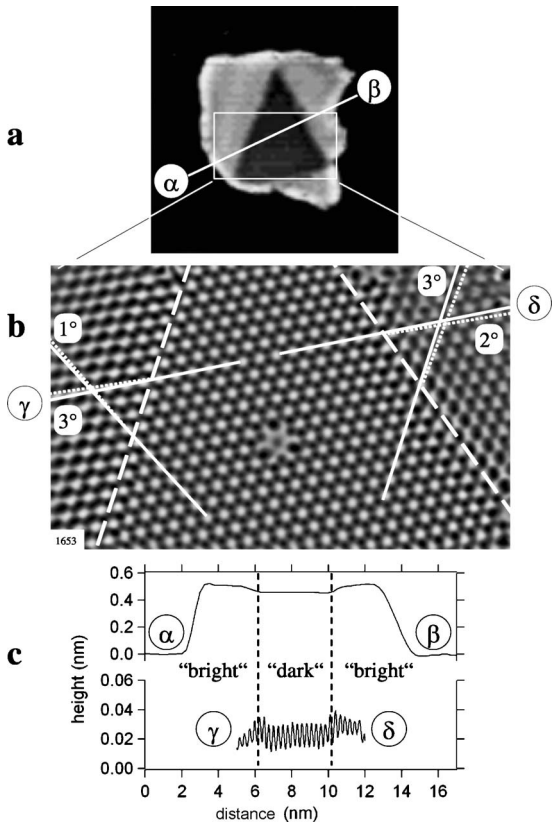

FIG. 4. (a) STM image of a bilayer island also shown in Figs. 3(b) and 3(c) (imaged at −0.1 V and 0.3 nA). (b) Contrast inverted and high-pass-filtered atomically resolved image of a large part of the island surface imaged at −0.5 mV and 0.3 nA. The "dark" phase in the center shows a perfect hexagonal symmetry indicative of the fcc (111) Fe phase. The "bright" phase shows also a nearly hexagonal surface structure but is misaligned by about 3° relative to the ideal fcc phase. (c) Line profiles of the raw STM images between points indicated by greek letters in the STM images above. The contrast between the "dark" fcc and "bright" phases strongly depends on the tunneling voltage (note the different height scales).

their size, a rough outline of the structural evolution is obtained [Fig. 3(c)]. Evidently the islands nucleate in the "bright" phase. The evolution towards larger islands branches into two types with the smaller islands becoming either higher or, alternatively, wider and developing the "dark" phase. The latter seems to suppress or at least delay the nucleation of the third layer, leading to a more layer-by-layer-like morphology.

The atomically resolved STM image in Fig. 4(b) unambiguously identifies the "dark" phase as ideal fcc with a perfectly hexagonal surface layer and a perfect threefold symmetry of the defect in the center. Also the appearance of the atoms exhibits perfect hexagonal symmetry in this area. In contrast, the atomic rows of the "bright" phase are misaligned by angles between 1° and 4°. These are small values compared to the 10.5° of the ideal bcc (110) surface. Nevertheless, the appearance of the atoms shows the twofold symmetry of a bcc (110) surface. We shall therefore resort to three types of experiments to show that this small misalignment is really only the "tip of the iceberg" and the structure of the "bright" phase is more close to the bcc phase as it may seem from the STM images presented so far: These three methods are (1) scanning tunneling spectroscopy, (2) H_2 dosing, and (3) STM imaging of boundaries between different domains of the "bright" phase.

2. STS of bilayer and pyramidal islands

Scanning tunneling spectroscopy of bcc (100) Fe surfaces and individual Fe atoms shows characteristic and pronounced $dI/dV(V)$ maxima close to the Fermi level: A sharp $3d$-$4p$-$4s$ surface resonance can be seen by STS on the bcc (100) Fe surface.[39,40]

We observe such sharp and strong resonances also on ultrathin Fe/Cu(111) films, which turn out to be very structure sensitive. We now exploit these spectroscopic "fingerprints" to show that the "bright" phases in the pyramidal islands and in the bilayer islands are closely related. The tunneling spectra in Fig. 5 show three different peaks characteristic for the Cu substrate, the "dark" fcc Fe phase and the "bright" Fe phase. The peaks of the spectra shown in Figs. 5(a) and 5(b) obtained on different films with different STM tip states (dif-

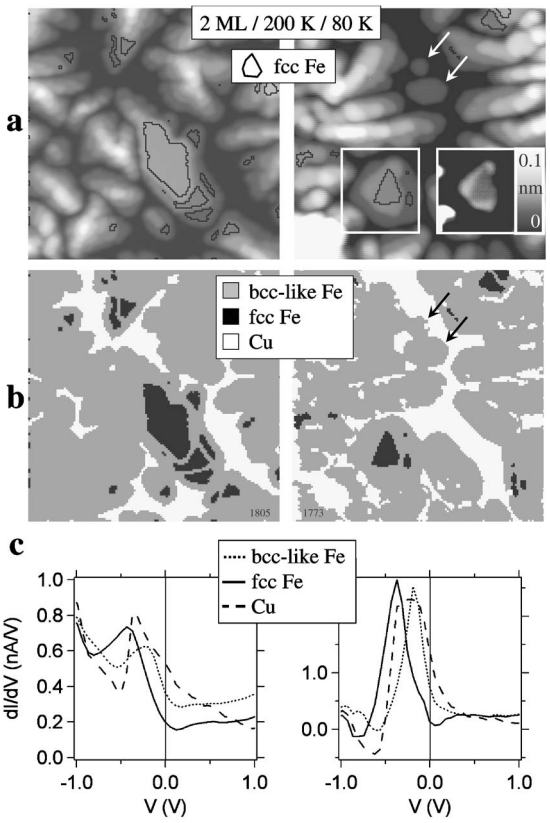

FIG. 5. Scanning tunneling spectroscopy of 2-ML films. Two different but equally prepared films are shown on the left- and right-hand sides. (a) Simultaneous STM images (50 nm wide, imaging at −1 V and 1 nA). The arrows indicate two single-phase bilayer islands. The white rectangle marks a trilayer island with coexisting fcc- and bcc-like phases. The inset is the same trilayer island with strongly enhanced contrast on the third atomic level. The black lines indicate regions identified as fcc by their spectroscopic "fingerprint" (cf. Sec. II). (b) Surface areas colored with respect to their spectroscopic fingerprint. (c) Spectra averaged over the areas shown in (b).

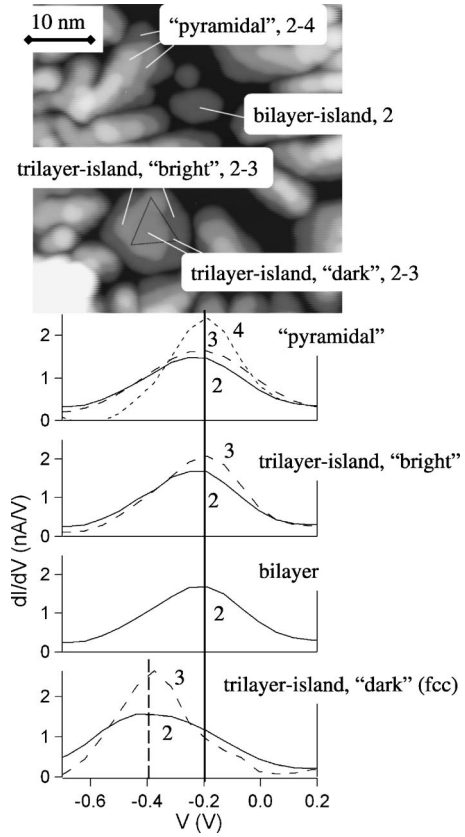

FIG. 6. Same spectroscopic data set as shown on the right-hand side of Fig. 5. Shown are tunneling spectra of islands of different sizes and morphologies near locations indicated in the simultaneously acquired STM image. The spectra are shown for each individual atomic level and in the case of the trilayer island also for "dark" fcc- and "bright" bcc-like regions within the same atomic level. The numbers inside the diagrams and the STM image indicate the local thickness in ML. The solid and dashed vertical lines indicate the location of the bcc-like and fcc-related peaks at −0.2 V and −0.4 V, respectively. With higher local thickness, the peaks both in fcc- and bcc-like regions very slightly shift to higher energies and become more intense and narrower.

ferent configurations of the atoms at the tip apex) have very different signal-to-background ratios but share the most important features. The Cu surface state shows a sharp onset and a slower decay towards higher energies characteristic of a 2D-delocalized free-electron-like electronic state.[41] The Fe surface states or resonances appear more peaklike similar to those on the bcc (100) surface.[39,40]

The Fe film shown in the example on the right-hand side of Fig. 5(b) shows a trilayer island with a triangular fcc area analogous to that visible on bilayer islands (cf. Fig. 4). The STS peak on the fcc domains in both examples is located 0.4 eV below the Fermi edge. Note that the fcc domains in Fig. 5(b) seem to be interrupted by step edges. This should not be taken too seriously as tunneling spectra taken at step edges are often ill defined and cannot be used to distinguish clearly between the two Fe phases.

The larger fraction of the Fe film shows a peak at 0.2 eV below the Fermi edge. Most of this majority fraction consists of pyramidal multilayer islands, which are known to be bcc or at least bcc-like from XPD measurements at 80 K.[16] There is no reason to assume that the temperature difference of 120 K to our growth temperature should change this. Therefore the STS peak measured on the pyramidal islands serves as a fingerprint for the bcc-like phase. We note that the cited XPD measurements[16] did not cover the entire hemisphere but are polar scans for a given azimuthal angle and are most certainly not very sensitive to strain in the bcc structure.

In order to analyze the tunneling spectra in dependence of the local film thickness and morphology we compare the spectra for each individual atomic level on the different island types in Fig. 6. The Fe peak positions in our spectra acquired at the location of the small bilayer islands, the "bright" parts of the trilayer island, and the "pyramidal" multilayer islands are almost identical and only weakly depend on the local thickness. The shapes of the spectra of a given level—e.g., the surface of the bilayer islands and the part of the trilayer or pyramidal islands where the second level is exposed—are nearly indistinguishable. This points to a very close relationship of the bcc-like structure of the pyramidal islands and the "bright" phase of the bilayer islands,

which we could atomically resolve (cf. Fig. 4). The significant broadening of the bcc-like peak of the bilayer level is not specific for the bcc-like phase, but can be seen also in the fcc bilayer spectrum.

3. Atomic model of the bilayer islands

The spectroscopic evidence together with the twofold appearance of the atoms and the misalignment of the atom rows in the high-resolution image (Fig. 4) suggests the classification of the "bright" phase as bcc (110)-like. This implies, as mentioned in Sec. III, a bridgelike stacking of the two Fe layers. In Sec. IV B 2 we will provide evidence for this type of stacking order by analyzing the atomic structure of a boundary between two bcc domains. For the time being, we use the assumption of a bridgelike stacking as a working hypothesis to construct our model of the bcc-like bilayer structure.

We observe that this bcc-like phase does not show a significant variation of apparent height, which would be indicative of severe lattice mismatch leading to a more or less periodic pattern of regions with energetically unfavorable on-top stacking (moiré pattern). Combining this absence of on-top stacking, the observed atomic positions, and the assumption of bridgelike stacking, we arrive at the atomic model shown in Fig. 7(a). The small misalignment of 3° observed in the bcc-like domain implies that the interface coordination (Fe layer on topmost Cu layer) changes continuously from fcc to hcp with increasing distance from the island center [Fig. 7(c)]. Despite this continuous change of the interfacial relationship, the boundary between the fcc and bcc-like phases is quite sharp. The line profiles α-β and γ-δ in Fig. 4(c) suggest an fcc-bcc domain boundary width of 2–4 interatomic distances. Figure 7(b) illustrates the different displacement directions of the Fe atoms at the interface in the two bcc-like "wings" to the left and right of the triangular fcc center region. The threefold symmetry of the substrate surface corresponds to three equivalent bcc-like domains, two of them visible in the STM image in Fig. 4 and shown in Fig. 7.

One might argue that the model in Fig. 7 also suggests a small kink in surface atom rows crossing the boundary between the fcc- and bcc-like domains of about 0.07 nm due to the different stacking of the two Fe layers. This is not observed. However, it is likely that the structure at the border is "smoothed" by various effects. For instance, the relative in-plane displacement of the two Fe layers necessary for the bcc-like bridge stacking is very likely distributed between the two layers, unlike in our simplified atomic model, thereby reducing the "kink" size on the surface to 0.035 nm of the interatomic distance by introducing a kink of similar size in the invisible interface Fe layer in the opposite direction. Other smoothing effects may include an electronic surface corrugation which is more regular than the positions of the atomic cores.

The nature of this particular type of lattice matching in the bcc-like domain implies that the size of a bcc-like domain is limited by an interfacial "no-on-top-site" constraint: Only Fe positions along the line connecting threefold fcc and threefold hcp substrate sites via bridge-site configurations are allowed [Fig. 7(c)]. For a 3° misalignment angle, a bcc-like strip of a width of 10–20 atom rows free of on-top stacking can form. Indeed, larger clean islands are never entirely in the bcc-like phase, which is limited to the outer parts of these islands [cf. Fig. 3(c)]. Therefore, a morphology with wide, flat islands clearly favors the fcc phase, while a high density of islands or holes in the film promotes the bcc-like phase.

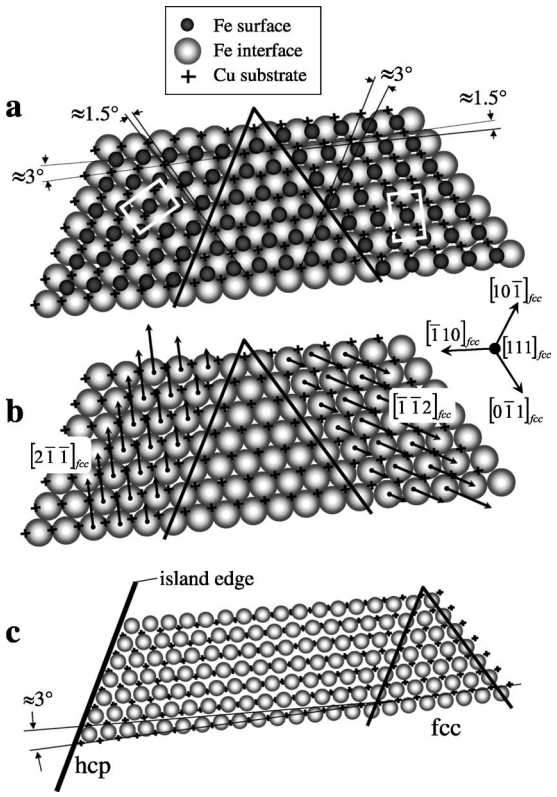

FIG. 7. Schematic model of the bilayer island shown in Fig. 4. (a) A bcc-like stacking of the two Fe layers and a "floating" fcc-to-hcp stacking at the Fe-Cu interface is proposed for the bcc-like "bright" domains, which are arranged around the triangular fcc kernel of the island. The rectangles indicate the bcc (110)-like unit cells of the differently oriented bcc-like domains. (b) Same model with surface Fe layer removed. The arrows indicate, strongly exaggerated, the displacements of the interface Fe atoms relative to the substrate fcc positions, which cause the 3° misalignment between the atom rows of the fcc and the bcc-like domains. (c) The relatively weak misalignment of 3° between the fcc substrate and bcc-like film avoids on-top coordinations at the Fe-Cu interface provided that the bcc-like regions are not wider than ≈20 atom rows.

Considering the 2D geometry of a single layer of the bcc-like bilayer structure, Fig. 8 shows that the 3° misalignment and the corresponding in-plane displacements of the atoms represent roughly 1/3 of the pathway towards the ideal Kurdjumov-Sachs-like oriented bcc (110) phase. This pathway breaks the 2D hexagonal symmetry of the surface layer but preserves in good approximation its 2D centered rectangular symmetry. Since thicker films grown at room temperature (cf. Sec. IV C) show a similar structure but 2/3 the way down the same pathway (7° misalignment) we term this phase KS-3° and the other phase KS-7°, accordingly. Again we emphasize that all evidence points to a bridgelike stack-

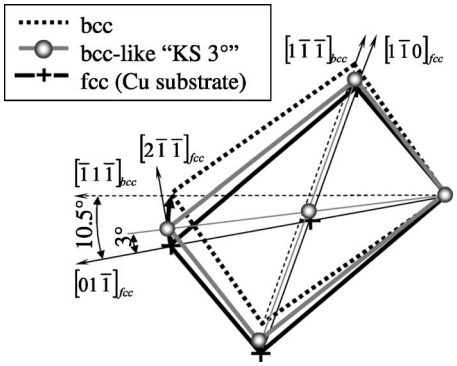

FIG. 8. In-plane atom arrangement in the observed bcc-like bilayer phase compared to the ideal bcc phase in Kurdjumov-Sachs orientation and the fcc phase. The characteristic misalignment of the observed bcc-like phase in the bilayer islands is only 3° instead of 10.5° for the ideal bcc phase, and the structure therefore labeled "KS-3°."

ing of the layers, which is the hallmark of the 3D bcc (110) structure. The observed atomic in-plane displacements serve as an indicator of the transformation but do not constitute the dominant deformation component.

B. H adsorption on bilayer islands at 80 K

1. Multidomain displacement vortices

Hydrogen adsorption has a substantial effect on the film structure, in particular on the "bright," bcc-like KS-3° phase. Storage of the sample inside the LN_2-cooled shields for significantly longer than a few hours at 80 K leads to characteristic contrast changes of the fcc and bcc-like phases. Since only hydrogen is present within the shields at 80 K with sufficiently high partial pressure, we attempted to reproduce the observed contamination-induced evolution of the island morphology by deliberate H_2 dosing. Indeed, the contrast changes in the STM images could be exactly reproduced (Fig. 9). We interpret these contrast changes as dissociative adsorption of H_2 on the film surface analogous to the adsorption on the (110) surface of an Fe single crystal.[42] Adsorption of relatively electronegative elements can lower the overall apparent height of the surface, as observed, e.g., for the C/Ni(100) system.[43,44] The difference in Pauling electronegativity between H and Fe is a little less than half of that between C and Ni.

The nine snapshots displayed in Fig. 9 are taken out of an image sequence acquired during dosing $\approx$25 L H_2 at 80 K. Initially adsorption shows an effect mainly on the "bright" bcc-like phase, which becomes quickly "noisy" and darker compared to the fcc phase, which remains almost unchanged (step 1, first contrast change). The noisiness points to a certain mobility of the H atoms, at least in the presence of the tunneling tip, before a sufficiently close packing of the H atoms on the surface is reached. Subsequently the now-darker H-covered bcc-like part of the film begins to expand until it has consumed most of the island area (step 2). Only after a dose of about 3 L does the small residual fcc center become again darker than the bcc-like phase, indicating increasing H coverage also there (step 3, second contrast change).

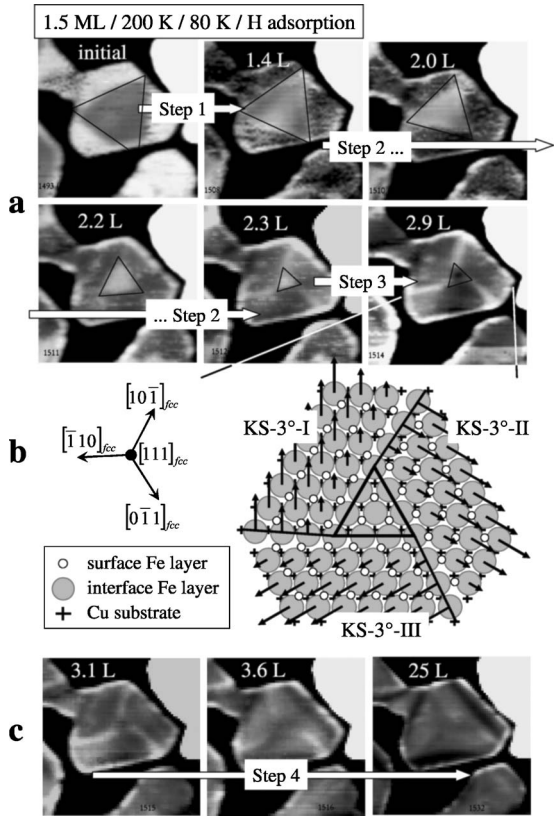

FIG. 9. H_2 adsorption on a triangular Fe bilayer island at 80 K. The image sequence shows four distinct steps of the structural modification (images 20 nm wide, tunneling at −0.22 V, 0.41 nA). (a) Steps 1–3. Step 1: the bcc-like phase is quickly covered with H and becomes dark (reduction of apparent height). Step 2: the bcc-like phase grows and the remaining fcc phase shrinks until nearly the entire island is bcc-like. Step 3: H adsorption shows an effect also on the (here tiny) fcc center triangle, which turns dark rather abruptly. (b) Schematic model of the bilayer film after adsorption step 3. The arrows indicate the displacements of the interface Fe atoms (exaggerated) relative to the substrate fcc positions. (c) Fourth and final step of H adsorption: The well-defined domain structure disappears, leaving diffuse darker and brighter areas.

The large difference in apparent H coverage between the different phases during the initial adsorption step provides additional evidence that the "bright" phase is not a marginally deformed fcc phase, but a bcc-like phase with a different layer stacking and therefore different electronic structure and adsorption properties. The direct origin of the high H occupancy of the surface sites on the bcc-like phase is most likely an adsorption enthalpy difference between the phases provided that the H atoms are sufficiently mobile (cf. previous paragraph). A different sticking coefficient or dissociation efficiency would be relevant only in the unlikely case of immobile H atoms at 80 K.

The domain structure resulting after completion of step 2 shows a threefold "pin wheel" symmetry (no reflection symmetry) in agreement with the structural models in Figs. 7 and 9(b). There are two possible shear directions differing by 120° for each of the three bcc-like domains. Minimization of

regions with compressive stress, however, aligns the directions for each pair of adjacent domains. Since the resulting shear strain—i.e., atom displacement pattern—endows the island with a rotational direction (chirality), we use the term "displacement vortex" for this domain arrangement. Consequently, two enantiomers (mirror images) of the vortex may form, one clockwise, the other counterclockwise oriented. To make things even more complicated, the fcc center triangle may also be twinned with respect to the surface plane with hcp-like stacking at the interface producing two more vortex subspecies. While the previous two examples (Figs. 4 and 9), are both clockwise oriented and regular fcc, the next example (Fig. 10) contains counterclockwise oriented, both fcc and twinned fcc vortices.

Figure 10 shows a larger bilayer island in a film grown at 300 K with the typical triangular fcc domain in the center. In this case H adsorption occurred inadvertently from the residual gas during 36 h of storage at 80 K inside the cryoshields of the STM. Since the structure is very similar to that seen after completion of "step 3" of the hydrogen-induced film transformation (Fig. 9) and no traces of other adsorbates like O or C can be found in the atomically resolved images, it can be safely assumed that the surface was exposed to an accumulated dose of ≈ 2 L or $\approx 2 \times 10^{-11}$ mbar average H_2 pressure during this period. Since clean bilayer films grown at 300 K are fully fcc, in this case the bcc-like phase is not only promoted but created in the H adsorption process at 80 K.

The hexagonal atomic pattern on the island surface [Fig. 10(b)] corresponds to a (2×2) superstructure. More precisely it is only nearly hexagonal since the sixfold symmetry is broken by a weak stripe pattern, which changes its orientation at every domain boundary [boxes with stripe pattern in Fig. 10(b)], and the atomic rows of the various domains are slightly tilted with respect to each other by about 1°–2°. In short, the surface structure is similar to that seen on the clean bilayer islands (Fig. 7), except that the bcc-like phases now cover a significant fraction of the islands. The origin of the striped corrugation component, which indicates the orientation of the bcc (110)-like domains is discussed in Sec. IV B 3 along with atomically resolved STM images.

This relatively large island shows a more complex domain structure, which is a consequence of the limited width allowed for individual bcc-like domains due to the "no-on-top-site" constraint at the Fe-Cu interface, but still can be broken down into individual displacement vortices [Figs. 10(c) and 10(d)]. In addition to the "main" vortex around the larger triangular fcc domain a second vortex with a smaller fcc center domain is formed with one of its surrounding bcc-like domains in common with the larger vortex structure. The incremental displacement of the interface Fe atoms in the bcc-like domain from fcc to hcp sites [cf. Fig. 7(c)] requires that the Fe atoms in the smaller fcc domain are placed in hcp-sites of the substrate. This in turn implies that the two Fe layers of the smaller fcc domain and the substrate layer are stacked like an fcc twin with respect to the substrate (sequence "*BAC*" instead of "*ABC*" with substrate layer "*C*").

However, the structure is not perfect and fails to avoid on-top-site-stacking at the Cu-Fe interface in the bright area of domain III in the lower left part of the island. This domain touches both the smaller (along its bottommost triangle side) and the larger vortex (at its bottommost triangle vertex). While the larger vortex dictates fcc stacking in this domain, the smaller vortex dictates hcp stacking in the same domain. The result of this frustration is a near on-top-stacking visible as increased apparent height near the larger fcc domain [star symbols in Figs. 10(b) and 10(d)].

Regarding an effect possibly relevant for higher H doses, we remark that the edge regions along two sides of the island [labeled (NW) in Fig. 10(b)] appear to constitute a more relaxed bcc-like structure in a Nishiyama-Wassermann configuration [cf. Fig. 1(a)]. Our image database, however, is too limited to allow a definite conclusion in this case. We also note that the displacement vortex structures described above are not the final state of the Fe film in the limit of high H coverage. Dosing H_2 beyond 2–3 L [Fig. 9(c)] apparently dissolves this domain structure, leaving complex-shaped wavy dark and bright regions (Fig. 9, step 4). Another characteristic of this last adsorption-induced transformation step is the appearance of dark, about 1 nm wide, paired dislocationlike lines in larger bilayer islands. Therefore experiments using H_2 doses higher than 2–3 L will very likely not arrive at the vortex structures shown above. This final transformation step requires further investigation, but is beyond the scope of this paper, which employs H adsorption mainly as a vehicle to improve the understanding of the clean Fe films.

2. Determination of the bilayer stacking by STM

So far the detailed atomic structure of the island has been inferred from the domain arrangement and the near atomic resolution of the H superstructure. Now an individual domain boundary is studied in detail. Figure 11(a) shows the same bilayer island as in Fig. 10 after repeated scanning. Obviously, the fcc region (dark triangular area in the center) has become slightly smaller while scanning. There is no indication, however, that the domain arrangement itself has changed. Since the two phases, fcc- and bcc-like, are in a subtle balance with respect to their domain size (cf. discussion Sec. V B), small shifts of the domain boundaries by forces applied to the metal atoms or due to redistribution of the H atoms by the tunneling tip are not surprising.

The STM image in Fig. 11(b) shows the atomically resolved surface atom lattice around the domain boundary which originates at the bottommost vertex of the larger triangular fcc domain. As Fig. 10(c) shows, our model suggests that this domain boundary is a "nonregular" one with a lower surface atom density compared to the other boundaries in Fig. 10(c). The STM image confirms this model, showing 3.5 rows of surface atoms on top of 4 rows of interface Fe atoms. The particular relative displacement of the surface atoms at both sides of the boundary [white circles in Fig. 10(c)] is fully consistent with our model based on a bcc-like stacking.

3. Tentative model for H superstructure

Although the argumentation above does not rely on a particular way how the H atoms decorate the three rotational domains, we briefly speculate on the H superstructure on the bilayer islands leading to the observed simultaneous (2×2)

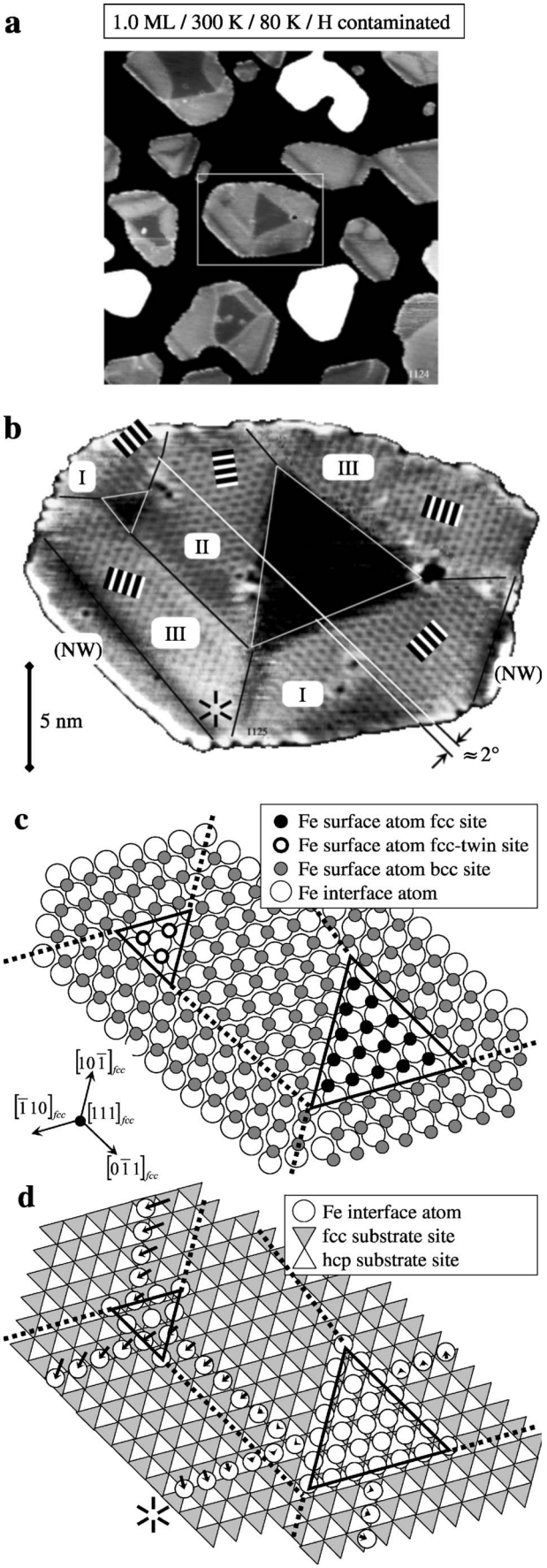

FIG. 10. Fe/Cu(111) film grown at 300 K after adsorption of ≈2 L H_2 from the residual gas. (a) Overview STM image (70 nm wide, −1 V, 1 nA) showing mainly bilayer islands. (b) Contrast-enhanced image of the multidomain bilayer island outlined in the overview image (−20 mV, 1.8 nA). The island surface shows a near-hexagonal atomic pattern indicative of a (2 × 2)-H superstructure decorating the three bcc-like rotational domains. The domain orientation becomes apparent as a weak stripe pattern with twice the periodicity of the Fe lattice, as indicated by the striped boxes. These rotational domains are arranged around the large triangle-shaped fcc Fe domain forming a displacement vortex like that shown in Fig. 9. The angular misalignment of ≈2° between domains I and II is indicated (cf. Figs. 4 and 7). A smaller second fcc domain with its own vortexlike environment is formed on the left-handside of the island with one domain (II) in common with the larger fcc domain. (c) Model of the film structure. Outside the two fcc center domains, the Fe layers are bcc like—i.e., bridge-site stacked. (d) Model of the film-substrate interface. The arrows indicate the displacement of the Fe atoms relative to the substrate's fcc positions (dark triangles). The star symbol close to the lower island edge marks a small region where the double vortex structure cannot avoid on-top stacking causing a large apparent height and therefore brighter appearance in the STM image in (b). The narrow edge domains marked (NW) may be relaxed bcc in Nishiyama-Wassermann orientation (see text).

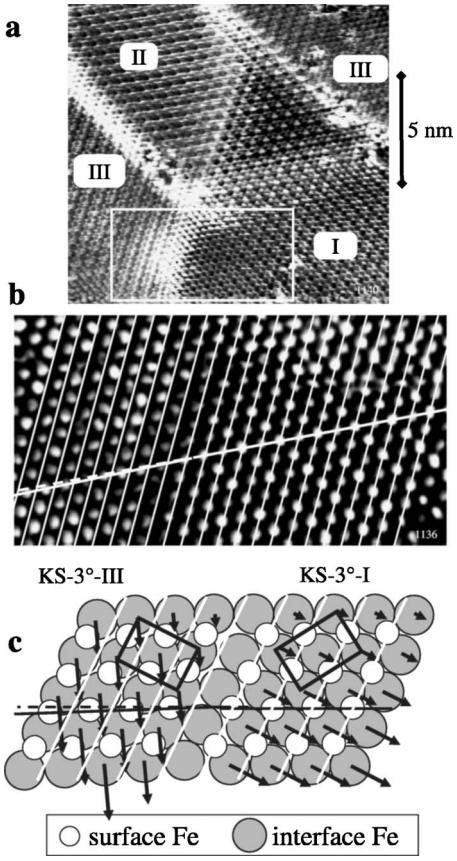

FIG. 11. (a) STM image of the same bilayer island as that shown in Fig. 10. During repeated scanning, the fcc center has become slightly smaller, although the overall domain arrangement remains unchanged (−1 mV/10 nA). (b) Atomically resolved area marked by the white rectangle in (a) (−1 mV, 9 nA). The atom displacements between the adjacent KS-3°-I and -III domains are demonstrated by the grid of equidistant lines and the individual line following an atom row across the boundary. (c) Schematic model with exaggerated displacements (arrows) of the interface Fe atoms relative to the fcc positions of the Cu substrate. Note that the Fe atom density of the surface layer is significantly reduced along the domain boundary.

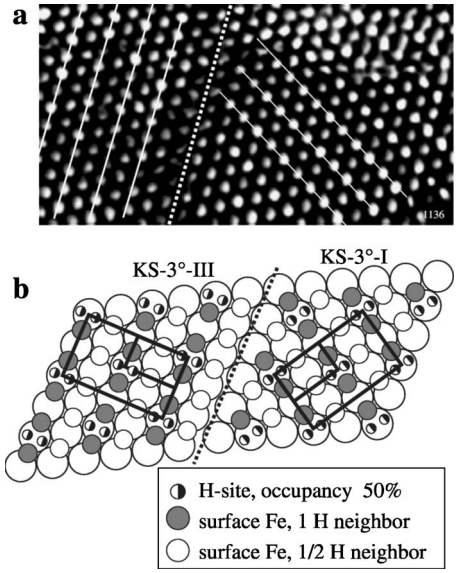

FIG. 12. (a) Same atomically resolved image as in Fig. 11. The solid white lines now mark rows of brighter atoms producing the "stripe" pattern visible in images with lower resolution [Fig. 10(b)]. The dotted line marks the approximate location of the domain boundary center. (b) Possible arrangement of the H atoms in analogy to the H superstructure on the bulk Fe(110) surface (Ref. 42), explaining the different apparent heights (brightnesses) of the metal atoms by their different (average) H coordination. The $c(2\times2)$-H superstructure unit cell and the strained bcc (110) unit cell are marked by the large and small rectangle, respectively.

pattern and stripe pattern with twice the substrate lattice periodicity. The atomically resolved image in Fig. 12 (same as in Fig. 11) shows that the origin of the stripes are rows of atoms slightly brighter than their neighboring rows.

The ≈3° shear deformation of the 2D in-plane film geometry breaks the 2D hexagonal symmetry but leaves the rectangular symmetry intact (cf. Fig. 8). This symmetry is exactly that of the ideal bcc (110) Fe surface and makes a direct comparison to the adsorption sites on (110)-oriented bulk Fe (Refs. 42 and 45) particularly compelling. LEED-I/V work on bcc Fe (Refs. 42 and 45) and a recent LEED-I/V study of ultrathin Fe films on Cu(100) (Ref. 46) suggest H positions either in threefold hollow or long-bridge sites. Even if a threefold equilibrium position is assumed, at sufficiently high temperatures the H atom may hop across the long-bridge site, creating a situation where the average position of the H atom is the long-bridge site.[42,45] We remark that the coverage in this study was 50%,[42,45] while the superstructure pattern observed by us on the bcc (110)—like bilayers on Cu(111) points to a coverage of only 25% as shown in the schematic Fig. 12(b).

If our model of the H superstructure is correct, the atomically resolved image shows only the effect of the H atoms on its metal neighbors, while the image acquired with higher tunneling resistance [Fig. 10(b)] shows additionally the H positions as corrugation minima.

C. fcc-bcc transformation in 3–4-ML films grown at 300 K

In 1–2 ML films grown at 300 K, we did not observe the "bright" bcc-like phase even in small islands, although in this case the analysis is more difficult because Cu segregation on top of the Fe film generates a "bright" phase of its own. However, Cu-covered "bright" parts are not restricted to the island edges but often cover whole island sections and show a more distinct contrast relative to the fcc Fe surface than the bcc-like KS-3° phase in films grown at 200 K.

As described in the previous sections, 1-ML films grown at 300 K are dominated by large fcc bilayer islands with a smaller island number density compared to films grown at 200 K [Fig. 2(b)]. In thicker films, the often triangular islands merge and form the base bilayer for a near layer-by-layer growth mode. The films still contain deep holes [Fig. 13(a)] probably because of the slightly smaller lattice constant of fcc Fe relative to Cu, which stabilizes the meandering canyonlike holes.[15] We remark that deep holes may also be created by Cu segregation[47,48] ["microscopic pinholes"

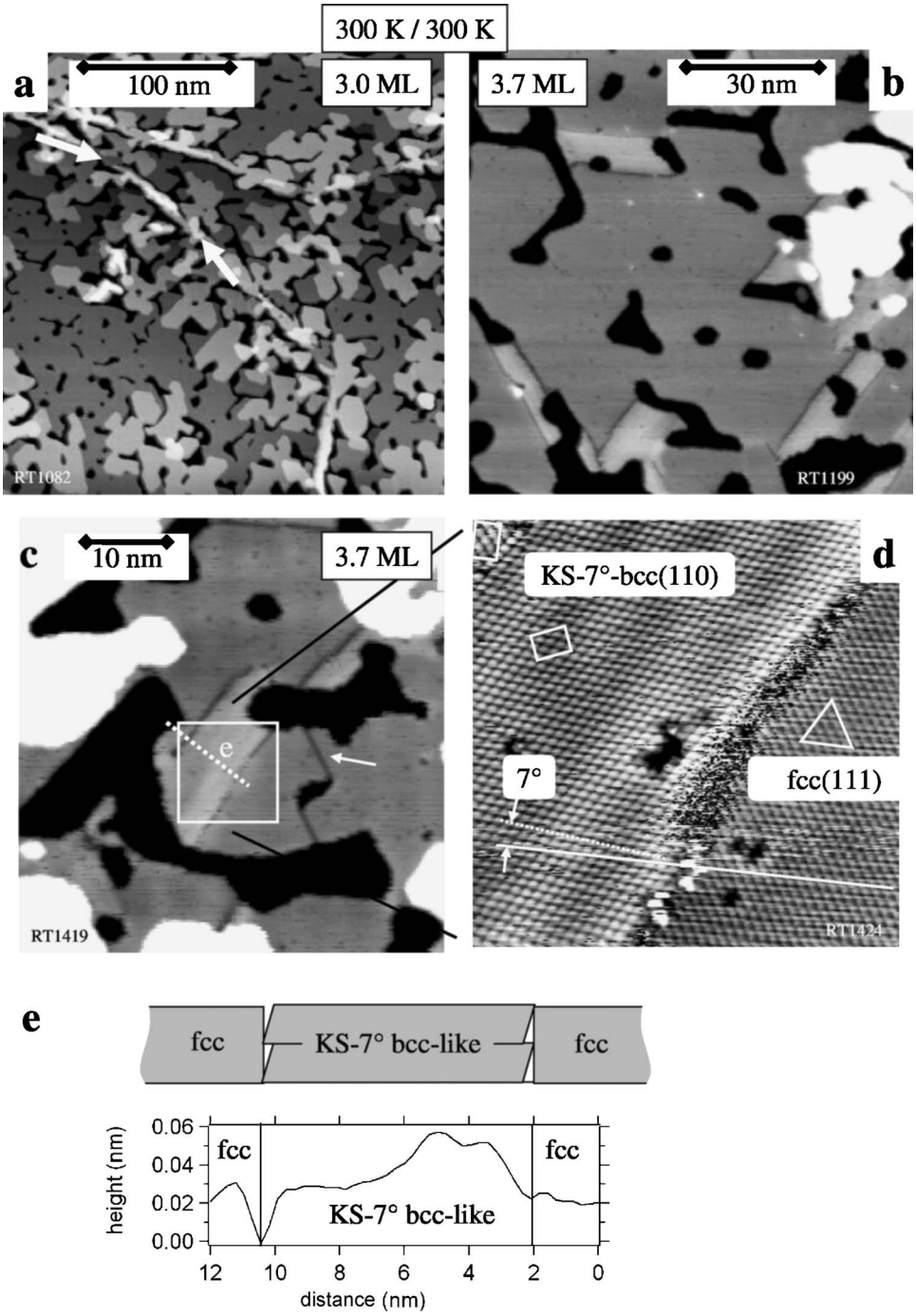

FIG. 13. STM images of 3.0 and 3.7 ML films grown and imaged at 300 K. (a) Overview image of a 3.0-ML film with substrate step edges decorated by elongated pyramidal ("ridgelike") islands (arrows). (b) Fourth ML of a 3.7-ML film with bcc-like regions appearing as bright stripes connecting deep holes in the film. (c) Individual bcc-like domain. The dark lines (arrow) are presumably boundaries between film regions, which are fcc twins with respect to each other. (d) Atomically resolved image of two grain boundaries between fcc- and bcc-like domains and between bcc-like reflection twins (upper left corner). The in-plane shear angle of this Kurdjumov-Sachs-like oriented bcc-like phase, termed "KS-7°," is typically 7° for a local thickness of 4 ML. (e) Schematic cross section illustrating the misalignment at the vertical interfaces between the bcc-like and fcc Fe phases. The line profile (location marked by dashed line in c) shows a distinct buckling at the right-hand side of the bcc-like grain, indicating lattice mismatch. Tunneling conditions: (a)–(c) −1 V, 1 nA; (d) −0.8 mV, 11 nA.

formed above ≈400 K in Co and Fe films on Cu(100)]. The hole density, however, is too high compared to the amount of Cu found on the surface (order of 10% or less), and the holes are not deep enough to qualify as such pinholes, which reach significantly below the substrate-film interface.[47,48]

Noncommensurate satellites in the LEED images of films more than 2 ML thick are indicative of bcc Fe in Kurdjumov-Sachs orientation (cf. Fig. 1). So far the location of these bcc regions was assigned to pyramidal ("ridgelike") film structures,[31] which at 300 K growth temperature form preferably along step edges [arrows in Fig. 13(a)]. In contrast, our STM images show that bcc regions can also form far from substrate step edges. They appear as brighter regions, apparently elevated by 0.01–0.04 nm [Fig. 13(b)] and are sometimes bordered by straight dark lines on one side. These lines are presumably incoherent twin boundaries and are present also in pure fcc regions of the film [arrow in Fig. 13(c)].[49] Such boundaries are known to separate twinned fcc regions from regular, substrate-oriented fcc regions.[49] Twinned fcc grains may nucleate due to hcp stacking of the initial monolayer (cf. Refs. 49 and 50 and "antiphase boundary" in Fig. 5 in Ref. 15). Indeed, the results of a quantitative photoelectron diffraction study by Theobald *et al.*[30] suggest that a fraction of about 10% of a 0.4-ML Fe film grown on Cu(111) at 300 K may be hcp stacked on the substrate. Boundaries between such fcc twins, which we observe in our

≈3-ML films, are high-energy defects like step edges and promote the nucleation of the bcc phase by facilitating shear deformations in the surface plane. However, low-temperature images suggest the presence of similar bcc domains also without nearby fcc-hcp fault planes, at least after cooling the film to 80 K.

Atomically resolved STM images [Fig. 13(d)] as well as LEED images show that the interrow distances of this bcc-like phase are almost that of ideal bcc Fe. The residual strain perpendicular to atom rows nearly parallel to the fcc-bcc domain boundaries (bcc ⟨112⟩– and fcc ⟨112⟩–type directions) is very small and ranges between 1% and 3% with smaller values for locally thicker films according to the position of the LEED satellites. Surprisingly, however, the Fe bond angle of the bcc-like phase in the surface plane amounts only to ≈67° instead of 70.5° required for ideal bcc. The possible origin of this shear strain (3.5° deviation from ideal bcc bond angle) is discussed in Sec. V.

The larger interrow distance on the surface compared to the substrate lattice requires that 1 or 2 atom rows be removed, if the martensitic transition occurs towards the end of the film growth or are not inserted during the film growth in the first place. Possibly related to this mass transport is the instability of the surface atoms at the fcc-bcc border which can be seen as image noise at low tunneling resistance [Fig. 13(d)]. Increasing the tunneling resistance diminishes the atomic resolution but leads to more stable imaging conditions at the fcc-bcc boundary. The mismatch effects due to the different atom density of film and substrate causes a weak corrugation of the film surface of about 30 pm on a length scale of 2–4 nm [line profile in Fig. 13(e)].

V. DISCUSSION

The experiments presented in this article cover two aspects of the Fe/Cu(111) films: First, the structure of a bcc-like phase in bilayer islands grown at 200 K. Second, the more "classic" problem of how and at which local thickness pseudomorphic fcc films grown at 300 K convert to bcc. The following discussion relates these results to recently published experiments with Fe/Cu(100) and Fe/Cu(111) films addressing structure and magnetism of these films, and to first principles calculations of the Fe/Cu(111) system.

A. Structure of the bcc-like phase in bilayer islands

The starting point of our discussion is the coexistence of two phases in bilayer islands grown at 200 K, which are easily identified by their different apparent heights in STM images. We can rule out that Cu is present on the surface at this temperature, which might also produce such a contrast in apparent height. Three groups of experimental results identify the phase with the larger apparent height ("bright" phase) as bcc like.

First, we use our scanning tunneling spectroscopy data to compare the electronic structure of the phase-mixed bilayer islands and the narrow single-phase pyramidal islands. Kief and Egelhoff[16–18] have shown by x-ray photoelectron diffraction that 80 K films are bcc-like already in the very initial phase of the film growth—i.e., at 1.1 ML average thickness. In films that we have grown at 90 K the entire Fe film consists of narrow pyramidal islands. We therefore use the pyramidal islands as a reference for the bcc-like phase in our local STS analysis. Indeed, the "bright" phase in the phase-mixed bilayer islands shows the same spectroscopic fingerprint as the pyramidal islands, which is a sharp peak at −0.2 eV in contrast to the fcc-like peak at −0.4 eV. We therefore conclude that the "bright" phase in question, which dominates in very small bilayer islands, but is restricted to the edges of larger bilayer islands, has a structure very close to bcc.

Second, the arrangement of the surface atoms in the "bright" phase as seen by STM does not show a threefold symmetry, regardless of the small size of the in-plane misalignment angle of only 3°. The stability of an fcc-like phase, which breaks the threefold fcc (111) surface symmetry—i.e., shows a distortion other than a modified interlayer distance or an isotropic volume change—is not plausible and unlikely to find theoretical justification. Such a model of a weakly distorted fcc phase proposed for the Fe/Cu(100) films[21] turned out to be unstable with respect to a bcc-like structure.[23] We emphasize again that although this weak in-plane deformation clearly indicates the presence of the bcc phase, it does not constitute the main deformation component of the fcc-to-bcc transformation. The main deformation is a change of layer stacking, which is only indirectly visible by STM.

Third, hydrogen adsorption alters the equilibrium between bcc-like and fcc phases to the point where the fcc phase almost disappears (possible explanation see next section). Since H adsorption does not increase the in-plane shear angle of about 3° in the bcc-like phase, we assume that the no-on-top-site rule for the stacking at the Cu-Fe interface is still valid and that the structure of the bcc-like phase has not significantly changed. A side effect of the H-induced larger bcc-like domains is more and longer domain boundaries between the bcc-like rotational domains, which can be imaged with atomic resolution. At such a domain boundary, we could observe a relative lateral displacement of the first-layer atoms that is characteristic for adjacent bridge-like stacked bcc (110)-like domains with different rotational orientation. This confirms our assumption of a bridgelike layer stacking.

Combining these three groups of results, we conclude that bilayer films with a sufficiently high step edge density, which facilitates in-plane atom displacements, may show a substantial bcc-like fraction, despite a nearly hexagonal in-plane atomic arrangement.

Concluding the discussion of the bilayer film structure, we comment on the observed apparent heights of the bcc-like and fcc phases. Based on the ideal geometry of a weakly strained, pseudomorphic fcc film, the interlayer distance of an ideal bcc (110) bilayer should be 6 pm per ML smaller (−3%) than that of an fcc (111) bilayer. In our STM images, the interlayer distance of the bcc-like phase appears to be at least 5 pm per ML larger (more than +2%) depending on the tunneling voltage. The observed discrepancy of more than 5% can be explained by the combined effect of the in-plane strain of the bcc-like Fe film accounting for +3% (cf. next section), by the mismatch at the Fe-Cu interface, and most

importantly by the difference in the electronic structure: At small but not too small tunneling voltages of approximately −0.1 V, the bcc-related surface state strongly contributes to the tunneling current, while the fcc-related one does not. This can be seen in the line profile α-β in Fig. 4(c) showing an apparent height of the bcc regions, which is up to 50 pm higher than the fcc regions. For images taken at −1 V or −0.5 mV [line profile γ-δ in Fig. 4(c)], the difference is much smaller, typically only 10–20 pm (5–10 pm per ML).

B. Stability of the bcc-like phase in bilayer islands

In order to justify our claim of a bcc-like phase compatible with the surface structure observed by STM, we now estimate the relative stability of this bcc-like phase compared to the fcc phase. The observed small in-plane misalignment angle of 3°, corresponding to an in-plane bond angle in the bcc-like phase of 63°, appears to be a trade-off between the strain in the bcc-like Fe film, which increases the total free energy of the system and the width of the bcc-like domain, which lowers it. We have estimated the strain energy for our structural model of the bcc-like phase using the experimental second- and third-order elastic constants.[51] The KS-3° phase can be formed from the bcc phase either by a strain with predominantly normal character (setup I: $x=[00\bar{1}]$, $y=[\bar{1}10]$, $z=[110]$): $\varepsilon_{xx}=-6.8\%$, $\varepsilon_{yy}=+7.5\%$, $\varepsilon_{zz}=+2.8\%$ or predominantly shear character as shown in Fig. 14 (setup II: $x=[\bar{1}1\bar{1}]$, $y=[\bar{1}12]$, $z=[110]$): $\varepsilon_{xx}=+2.9\%$, $\varepsilon_{yy}=-2.5\%$, $\varepsilon_{zz}=+2.8\%$, $\varepsilon_{xy}=-13.0\%$. Both pathways differ only by a small rigid rotation. The corresponding elastic energy per atom, using the initial atom volume Ω, $\Omega(C_{ijkl}\varepsilon_{ij}\varepsilon_{kl}/2+C_{ijklmn}\varepsilon_{ij}\varepsilon_{kl}\varepsilon_{mn}/6)$,[51] is ≈50 meV/atom with less than 10% of this value in the third-order terms. Note that the strain ε_{zz} (relative increase of interlayer distance) is a result of the assumption of a free surface and leads to a volume increase of the bcc-like phase of ≈3% (compared to ideal bcc). Since the interlayer distance of ideal bcc (110) Fe is ≈3% smaller than that of the fcc (111) film to begin with, the resulting interlayer distance of the bcc-like KS-3° phase is virtually identical to that of the fcc (111) phase.

The value for the elastic strain energy E_{strain} of only 50 meV/atom in the bcc-like domain is surprisingly small and shows that the observed in-plane distortion contains relatively little strain energy, if the correct—i.e., bridgelike—layer stacking is assumed. One might think that this elastic energy has to be balanced by an at least equally large transformation energy per atom $E_{fcc\text{-}bcc}$ (defined between ideal fcc and bcc). However, there is a domain size dependence of the strain in the bcc-like domains, which requires that $E_{fcc\text{-}bcc}$ be significantly larger than E_{strain}: If the "no-on-top-site" condition is observed, a narrower domain can relax more towards the ideal bcc structure and still avoid on-top site configurations and a wider domain less [cf. Fig. 7(c)]. This limits the equilibrium domain width: A bcc-like domain can grow only to the point where the energy loss due to strain equals the gain in transformation energy. The total transformation energy will be approximately linear with the domain volume—i.e., domain width. The strain energy will rise faster because not only the volume but also the strain itself increases with

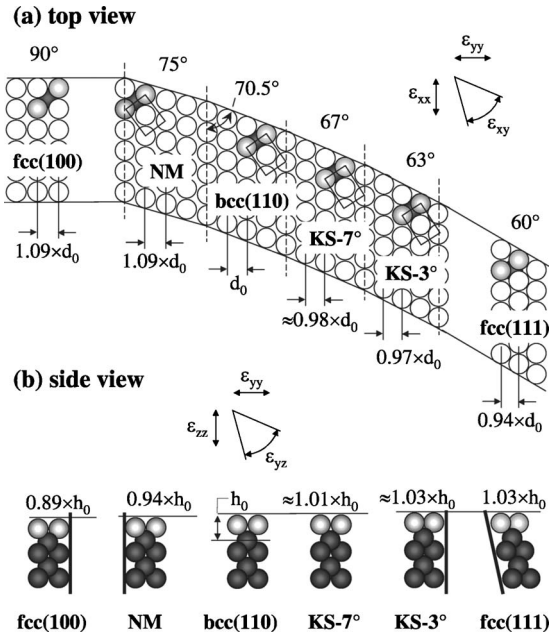

FIG. 14. Illustration of the four bcc (110)-like phases observed in the systems Fe/Cu(100) and Fe/Cu(111) in relation to the fcc (100) and fcc (111) phases. The acronym NM stands both for the nanomartensite phase (Ref. 27) and the bcc-like needle-crystals (Ref. 26) in Fe/Cu(100) films, while KS-3° and KS-7° are the two Kurdjumov-Sachs-like phases in Fe/Cu(111) films. The directions and orientations of the different components of the strain-tensor ε_{ij} are shown both in the top view of the surface and the cross section parallel to the yz plane. (a) Top view: the in-plane bond angles in nearest-neighbor atom triples are indicated. The stacking order of the phases is indicated by a representative atom in the adjacent atomic layer below. The observed interrow distances relative to that of the bcc (110) phase (d_0) is shown below. (b) Side view: the interlayer distance relative to that of the bcc (110) phase (h_0) is indicated. The value for the NM phase is taken from LEED experiments (e.g., Ref. 6), while those of the KS-3° and KS-7° structures are our estimates based on third-order elastic theory. The thick (near) vertical lines illustrate the perfect lattice matching between fcc (100) and NM phases and the imperfect lattice matching between fcc (111) and the KS phases. Note that while all other phases exist in films locally at least up to 8 monolayers thick, the KS-3° phase was observed only in bilayers although shown here 5 ML thick for the purpose of comparison.

increasing domain width. Therefore, a minimization of the total energy with respect to the domain width will result in an optimum width at a strain energy per atom, E_{strain}, which is lower than $E_{fcc\text{-}bcc}$. The simplest model consists of a bcc-like domain at the edge of a semi-infinite Fe bilayer and assumes a quadratic dependence of the elastic energy on the shear strain. The resulting equilibrium ratio between transformation energy and strain energy per atom then becomes $(\alpha_0+\alpha)/(\alpha_0-\alpha)\approx 2$ using the maximum misalignment angle $\alpha_0=10.5°$ for relaxed bcc Fe and the observed angle of $\alpha=3°$ for the KS-3° phase. Thus, the transformation energy $E_{fcc\text{-}bcc}$ in our case must be at least about 100 meV/atom. This is higher than the value expected for the transformation free energy of bulk Fe [60 meV/atom (Ref. 29)]. However, previous Fe/Cu(100) film experiments suggest that, for films

only a few ML thick, this value may be significantly increased due to surface effects.[28]

H adsorption, however, seems to increase the driving force sufficiently to convert also larger islands almost entirely into the bcc-like phase. This does not require as much energy as one might expect because the domain width of an already strongly strained phase like the KS-3° phase can be increased significantly by a relatively small decrease of the bond angle and a correspondingly small increase of the strain energy. Since the in-plane bond angle and the domain width are indirectly proportional to each other if the "no-on-top-site" constraint is observed, a width increase by a factor of 2 requires a decrease of the bond angle by only 1.5°. This relatively indifferent equilibrium between the bcc and fcc phases provides a plausible explanation for the dramatic effect of the H adsorption on the size of the bcc-like domains.

In this context it is interesting to note that H adsorption increases ferromagnetism in Fe/Cu(100) films in the thickness range of 4–5 ML,[52] where the film is highly unstable with respect to its structure.[27,28] Since ferromagnetism and bcc-like structure are clearly linked,[28] this H-induced magnetization increase indicates a bcc-stabilizing effect of hydrogen adsorption also in the Fe/Cu(100) system.

C. Structure of the bcc-like phase in 3-ML films grown at 300 K

We now briefly discuss the initial stages of the fcc-bcc transformation of films grown at 300 K and the differences of the resulting bcc-like phase to the KS-3° phase discussed in the previous sections. At 300 K, bcc-like domains are virtually absent in bilayer islands. This absence is presumably due to a reduced driving force towards the bcc phase (transformation free energy) at higher temperatures. If the local thickness reaches 4 ML, bcc-like domains are stable also at 300 K. A remarkable observation is the occurrence of these bcc-like domains also in flat parts of the film and not only in the pyramidal ("ridgelike") structures as previously suggested.[31]

Figure 14 shows this phase in relation to the other bcc-like phases observed. The misalignment angle between close-packed rows in the fcc (111) and bcc-like phases of 7° is the most prominent feature and this bcc-like phase correspondingly termed "KS-7°." This angle corresponds to a bond angle of 67°, which is different both from the 63° of the KS-3° phase but also from the 70.5° of ideal bcc Fe. Clearly, the interface-induced shear strain—i.e., the "no-on-top-site" condition—which keeps the misalignment angle small in bilayer films (KS-3° phase), is strongly reduced in the KS-7° phase.

Answering the question why the angle is still smaller compared to the ideal bcc phase is more complicated. In general, the reason is residual strain in the bcc-like domains caused by the surrounding fcc domains and the substrate. In the Fe/Cu(100) system, the strain state is mainly two dimensional: The bcc (110)-like phase forms without any significant mass transfer causing an interrow distance in the Fe film, which is commensurate to the Cu(100) substrate and therefore larger than that of ideal bcc Fe. This implies a large tensile normal strain in the bcc-like film, causing a shear strain, which is equivalent to an increase of the in-plane bond angle from 70.5° to 75° (cf. Fig. 14). Note that because of the particular symmetry, strains ε_{zx} and ε_{yz} are identical zero in Fe/Cu(100) films and vertical interfaces between fcc- and bcc-like Fe are perfectly lattice matched [left-hand side of Fig. 14(b)].

In the Fe/Cu(111) system, the bcc domains change their stacking while the fcc regions do not. This incompatibility implies that the vertical interfaces between fcc and bcc Fe are highly imperfect [cf. Fig. 13(e) and right-hand side of Fig. 14(b)], which most certainly causes out-of-plane shear strains ε_{zx} and ε_{yz} of unknown magnitude in the bcc domains and their fcc vicinity. Checking the interrow distance of the KS-7° phase (cf. Fig. 14) reveals that the atom row spacing at the surface is not commensurate to Cu(111) in this case, but close to that of ideal bcc Fe. Therefore also the normal strain ε_{yy} is not as well defined as in the Fe/Cu(100) system. Calculations using third-order elasticity theory indicate that both weak residual compressive normal strain ε_{yy} and weak out-of-plane shear strain ε_{yz} can contribute to the bond angle change from 70.5° to 67° as observed.

The high energetic cost of the imperfect vertical fcc-bcc interfaces also prohibits the formation of bcc grains narrower than 10–20 atom rows. In contrast, in Fe/Cu(100) films, where the vertical interface planes of the bcc-like domains are perfectly matched to the fcc lattice, isolated bcc grains may be as narrow as 8 atom rows in 6-ML films.[26]

D. Correlation of film structure with published magnetization data

In our model the observed film magnetization reflects the film fraction that is bcc-like and therefore shows ferromagnetism and a high magnetic moment—i.e., contains the KS-3° phase, the KS-7° phase, or a bcc-like phase[16–18] in a yet-unidentified strain state in the pyramidal islands. However, the strongly temperature-dependent morphology of the thermally grown films and the lack of detailed temperature-dependent magnetic and structural data prevents a quantitative correlation of structure and independently measured magnetization for this system. In addition, the thermally grown Fe/Cu(111) films are morphologically different from Fe/Cu(111) films prepared by pulsed-laser deposition[31,33,34] or those grown on stepped substrates.[53,54] Nevertheless, our model does provide a detailed view regarding the spectrum of strained bcc phases possible in these films and can explain the observed magnetization in TD and PLD films at least qualitatively:

(1) The increased stability of the bcc-like phase in small islands grown at 200 K as observed by us may help to resolve the low-coverage paradox observed in PLD films.[31,34] The magnetization is zero at 0.5 ML thickness, appears at 1 ML, and remains high up to 2.8 ML and drops rather suddenly to a smaller value above 2.8 ML.[31,34] In our scenario, the magnetization at low coverage is related to the bilayer and trilayer bcc-like "bright" KS-3° phase facilitated by the relatively high density of narrow islands and holes in PLD films below 3 ML thickness.[33] This is consistent with the

observation that the magnetic response appears at the beginning of the second monolayer,[31,34] when the first regions with a local thickness of 2 ML form. Since the third-layer islands are already significantly larger than the second-layer islands,[33] the KS-3° phase is more and more replaced by the fcc phase causing the drop of the magnetization [cf. Fig. 3(c)]. In addition, a finite thickness effect stabilizing the bcc-like phase below 3–4 ML local thickness, as observed in the Fe/Cu(100) films,[27,28] may further accelerate the destabilization of the bcc phase when increasing the thickness above 3–4 ML.

(2) A similar effect seems to occur in the films thermally grown on a stepped Cu(111) substrate at 280 K, which have been studied by x-ray magnetic circular dichroism.[54] At 0.8 ML the average spin moment is reduced from 3/4 of the bcc bulk value to 1/3. At this thickness threshold, the Fe bilayer island chains, which preferentially grow along the 10 nm spaced step edges, are on average 4 nm wide and start to coalesce. This sudden increase of the island size around 1 ML thickness leads to a strong reduction of the bcc-like fraction just as in the PLD films at 2–3 ML thickness.

(3) The magnetization of films thermally deposited at 220 K on a flat substrate, which should be comparable to the films presented in this work, slowly increases up to 2 ML thickness with increasing thickness, then increases rapidly up to 4 ML thickness, and finally shows the expected linear increase for bcc films at even higher thicknesses.[31,34] The low initial values of the magnetization below 2 ML thickness have previously been interpreted as a low-moment fcc phase.[31,34]

Applying our bcc-like model, the small magnetization value seems to be at variance with the relatively high bcc content observed by us (cf. Figs. 3 and 5). However, the fcc content in this temperature range is very temperature dependent. In the temperature range between 200 and 300 K, the morphology of the films changes from predominantly pyramidal (bcc-like) to predominantly bilayer and trilayer (fcc). Therefore an increase of the growth temperature by a few tens of K can significantly reduce the bcc content in favor of the fcc phase. Indeed the STM images of films directly corresponding to the magnetic measurements (cf. 2-ML TD film grown at 220 K in Fig. 1 in Ref. 31) show a dominant fcc-like morphology—i.e., wide islands mostly 2–4 monolayers high and much fewer pyramidal ("ridge"-like) islands as in our images (cf. 2 ML film grown at 200 K in Fig. 5). We therefore attribute the weak magnetization observed in these particular films[31] mainly to the pyramidal islands and a small density of KS-3° domains and the rapid increase of the magnetization above 2 ML to the formation of bcc-like KS-7° regions in the wide fcc islands as described in Sec. IV C.

E. Comparison with published first-principles calculations

For a magnetic and allotropic element like Fe, the search for the ground-state structure is particularly challenging due to the large number of possibilities for the combined magnetic and geometric structure. Recent calculations of the Fe/Cu(111) system[24] favor an fcc-like structure with (100) oriented bilayer-antiferromagnetic (BAFM) order—i.e., alternating two (100) layers spin up and two layers spin down—independent of the film thickness. Calculations presuming a ferromagnetic fcc phase result in a stable phase in a 2-ML film but show that 4-ML films are unstable with respect to monoclinic shear. In both cases, however, the ferromagnetic films are, if only slightly, higher in energy than the BAFM ones.

However, while these calculations of the Fe/Cu(111) system are meaningful for the fcc-like phase, they should not be directly compared to our bcc-like structural models derived from experiment. First, our model includes, besides a shear strain relative to the fcc lattice (monoclinic shearing) that is smaller than that assumed in the calculation,[24] also weak in-plane normal strains relative to the fcc lattice, which reduce the lattice strain in the resulting bcc-like film and improve the lattice matching at the interface between bcc-like film and substrate. Second, the change of the layer stacking, which we consider essential for the formation of a bcc (110)-like phase from an fcc (111) phase, was not explicitly included in the structural search in Ref. 24.

VI. SUMMARY

A detailed understanding of the crystal and domain structure of Fe/Cu(111) films grown at 200 K by thermal deposition is possible only with our model of bcc-like phases coexisting with the fcc phase. Small Fe bilayer islands grown at 200 K and imaged at 80 K are bcc-like up to a width of ≈5 nm. Larger bilayer islands are fcc with bcc-like domains at the island edges.

The atom rows in the bcc-like domains are misaligned to those of the fcc phase by about 3° and their spacing is slightly increased. The layer stacking in the bilayer is bcc like (bridge-site stacking), which is very different from the stacking in the fcc phase (threefold-hollow-site stacking). The transformation proceeds along a pathway leading to the Kurdjumov-Sachs orientational relationship ("KS-3°" phase), facilitated by the increased freedom for lateral atom displacements near step edges. The limited size of the lattice-misaligned bcc-like domains can be explained by the avoidance of on-top stacking at the interface. The bcc-like fraction can be increased substantially by adsorption of hydrogen at 80 K, leading to complex bcc-like multidomain structures also in larger bilayer islands grown at 300 K.

We suggest that the weak magnetization recently measured in thermally deposited films at 220 K (Ref. 31) corresponds to a small bcc-like film fraction in a predominantly fcc film. Moreover, we propose that the nearly linear increase of the strong magnetization below 2 ML thickness observed in PLD films grown at 220 K (Ref. 31) corresponds to a large bcc-like fraction stabilized by a high density of small islands and holes.

Films grown at 300 K form a bcc-like phase only above a local thickness of 4 ML. This phase is incommensurate to the fcc substrate lattice but shows an in-plane bond angle which

is still 3.5° less than that of the ideal bcc phase, indicating residual strain in the film. Domains of this "KS-7°" phase initially form on terraces between holes in the film or in sufficiently narrow islands.

ACKNOWLEDGMENT

We gratefully acknowledge support by the Austrian Science Fund (FWF).

[1] W. Keune, R. Halbauer, U. Gonser, J. Lauer, and D. L. Williamson, J. Appl. Phys. **48**, 2976 (1977).
[2] W. Becker, H. D. Pfannes, and W. Keune, J. Magn. Magn. Mater. **35**, 53 (1983).
[3] J. Thomassen, F. May, B. Feldmann, M. Wuttig, and H. Ibach, Phys. Rev. Lett. **69**, 3831 (1992).
[4] D. Pescia, M. Stampanoni, G. L. Bona, A. Vaterlaus, R. F. Willis, and F. Meier, Phys. Rev. Lett. **58**, 2126 (1987).
[5] A. Clarke, P. J. Rous, M. Arnott, G. Jennings, and R. F. Willis, Surf. Sci. **192**, L843 (1987).
[6] S. Müller, P. Bayer, C. Reischl, K. Heinz, B. Feldmann, H. Zillgen, and M. Wuttig, Phys. Rev. Lett. **74**, 765 (1995).
[7] D. Li, M. Freitag, J. Pearson, Z. Q. Qiu, and S. D. Bader, Phys. Rev. Lett. **72**, 3112 (1994).
[8] H. Zillgen, B. Feldmann, and M. Wuttig, Surf. Sci. **321**, 32 (1994).
[9] T. Detzel, M. Vonbank, M. Donath, and V. Dose, J. Magn. Magn. Mater. **147**, L1 (1995).
[10] T. Detzel, M. Vonbank, M. Donath, N. Memmel, and V. Dose, J. Magn. Magn. Mater. **152**, 287 (1996).
[11] J. Giergiel, J. Shen, J. Woltersdorf, A. Kirilyuk, and J. Kirschner, Phys. Rev. B **52**, 8528 (1995).
[12] K. Kalki, D. D. Chambliss, K. E. Johnson, R. J. Wilson, and S. Chiang, Phys. Rev. B **48**, R18344 (1993).
[13] U. Gradmann and P. Tillmanns, Phys. Status Solidi A **44**, 539 (1977).
[14] U. Gradmann and H. O. Isbert, J. Magn. Magn. Mater. **15**, 1109 (1980).
[15] A. Brodde and H. Neddermeyer, Ultramicroscopy **42**, 556 (1992).
[16] M. T. Kief and W. F. Egelhoff Jr., Phys. Rev. B **47**, 10785 (1993).
[17] M. T. Kief and W. F. Egelhoff Jr., J. Vac. Sci. Technol. A **11**, 1661 (1993).
[18] M. T. Kief and W. F. Egelhoff Jr., J. Appl. Phys. **73**, 6195 (1993).
[19] V. L. Moruzzi, P. M. Marcus, K. Schwarz, and P. Mohn, Phys. Rev. B **34**, 1784 (1986).
[20] V. L. Moruzzi, P. M. Marcus, and J. Kübler, Phys. Rev. B **39**, 6957 (1989).
[21] E. G. Moroni, G. Kresse, J. Hafner, and J. Furthmüller, Phys. Rev. B **56**, 15629 (1997).
[22] D. Spišák and J. Hafner, Phys. Rev. B **61**, 16129 (2000).
[23] D. Spišák and J. Hafner, Phys. Rev. Lett. **88**, 056101 (2002).
[24] D. Spišák and J. Hafner, Phys. Rev. B **67**, 134434 (2003).
[25] L. Kaufman, E. Clougherty, and R. J. Weiss, Acta Metall. **11**, 323 (1963).
[26] A. Biedermann, M. Schmid, and P. Varga, Phys. Rev. Lett. **86**, 464 (2001).
[27] A. Biedermann, R. Tscheließnig, M. Schmid, and P. Varga, Phys. Rev. Lett. **87**, 086103 (2001).
[28] A. Biedermann, R. Tscheließnig, M. Schmid, and P. Varga, Appl. Phys. A: Mater. Sci. Process. **78**, 807 (2004).
[29] G. L. Krasko and G. B. Olson, Phys. Rev. B **40**, 11536 (1989).
[30] A. Theobald, O. Schaff, C. J. Hirschmugl, V. Fernandez, K.-M. Schindler, M. Polcik, A. M. Bradshaw, and D. P. Woodruff, Phys. Rev. B **59**, 2313 (1999).
[31] P. Ohresser, J. Shen, J. Barthel, M. Zheng, C. V. Mohan, M. Klaua, and J. Kirschner, Phys. Rev. B **59**, 3696 (1999).
[32] J. Shen, Z. Gai, and J. Kirschner, Surf. Sci. Rep. **52**, 163 (2004).
[33] H. Schiechl, G. Rauchbauer, A. Biedermann, M. Schmid, and P. Varga, Surf. Sci. **594**, 120 (2005).
[34] J. Shen, P. Ohresser, C. V. Mohan, M. Klaua, J. Barthel, and J. Kirschner, Phys. Rev. Lett. **80**, 1980 (1998).
[35] P. J. Cumpson and M. P. Seah, Surf. Interface Anal. **25**, 430 (1997).
[36] W. Hofer, J. Redinger, A. Biedermann, and P. Varga, Surf. Sci. **466**, L795 (2000).
[37] G. Kurdjumov and G. Sachs, Z. Phys. **64**, 325 (1930).
[38] Z. Nishiyama, Sci. Rep. Tohoku Imp. Univ., Ser. 1 **23**, 637 (1934).
[39] J. A. Stroscio, D. T. Pierce, A. Davies, R. J. Celotta, and M. Weinert, Phys. Rev. Lett. **75**, 2960 (1995).
[40] A. Biedermann, O. Genser, W. Hebenstreit, M. Schmid, J. Redinger, R. Podloucky, and P. Varga, Phys. Rev. Lett. **76**, 4179 (1996).
[41] S. D. Kevan, Phys. Rev. Lett. **50**, 526 (1983).
[42] W. Nichtl-Pecher, J. Gossmann, L. Hammer, K. Heinz, and K. Müller, J. Vac. Sci. Technol. A **10**, 501 (1992).
[43] M. Schmid, A. Biedermann, and P. Varga, Surf. Sci. Lett. **294**, L952 (1993).
[44] C. Klink, L. Olesen, F. Besenbacher, I. Stensgaard, E. Laegsgaard, and N. D. Lang, Phys. Rev. Lett. **71**, 4350 (1993).
[45] L. Hammer, H. Landskron, W. Nichtl-Pecher, A. Fricke, K. Heinz, and K. Müller, Phys. Rev. B **47**, 15969 (1993).
[46] A. Biedermann, R. Tscheließnig, C. Klein, M. Schmid, and P. Varga, Surf. Sci. **563**, 110 (2004).
[47] A. K. Schmid, D. Atlan, H. Itoh, B. Heinrich, T. Ichinokawa, and J. Kirschner, Phys. Rev. B **48**, R2855 (1993).
[48] J. Shen, J. Giergiel, A. K. Schmidt, and J. Kirschner, Surf. Sci. **328**, 32 (1995).
[49] C. Busse, C. Polop, M. Müller, K. Albe, U. Linke, and T. Michely, Phys. Rev. Lett. **91**, 056103 (2003).
[50] C. Busse and T. Michely, Surf. Sci. **552**, 281 (2004).
[51] A. G. Every and A. K. McCurdy, in *High and Low Frequency Properties of Dielectric Crystals*, edited by D. Nelson, Landolt-Börnstein, New Series, Group III, Vol. 29, pt. a (Springer, Berlin, 1992), p. 635.
[52] R. Vollmer and J. Kirschner, Phys. Rev. B **61**, 4146 (2000).
[53] J. Shen, M. Klaua, P. Ohresser, H. Jenniches, J. Barthel, C. V. Mohan, and J. Kirschner, Phys. Rev. B **56**, 11134 (1997).
[54] P. Ohresser, G. Ghiringhelli, O. Tjernberg, N. B. Brookes, and M. Finazzi, Phys. Rev. B **62**, 5803 (2000).